

Antimicrobial activity of graphene oxide-metal hybrids

K. A. Whitehead,^{a*} M. Vaidya^a, C. M. Liauw^a, D. A. C. Brownson^b, P. Ramalingam^{b,c}, J. Kamieniak,^b S. J. Rowley-Neale^b, L. A. Tetlow^a, J. S. T. Wilson-Nieuwenhuis^a, D. Brown^a, A. J. McBain^d, J. Kulandaivel^c and C. E. Banks^{a,b}

^a School of Healthcare Science, Manchester Metropolitan University, Chester Street, Manchester M1 5GD UK

^b Faculty of Science and Engineering, Manchester Metropolitan University, Manchester, Chester Street, M1 5GD UK

^c Centre for Nanoscience and Nanotechnology, School of Physics, Bharathidasan University, Tamil Nadu, 620024, India

^d Faculty of Biology, Medicine and Health, University of Manchester, Manchester, M13 9PT UK

Abstract

With resistant bacteria on the increase, there is a need for new combinations of antimicrobials / biocidal agents to help control the transmission of such microorganisms. Particulate forms of graphite, graphene oxide (GO) and metal-hybrid compounds (silver-graphene oxide (AgGO) and zinc oxide graphene oxide (ZnOGO)) were fabricated and characterised. X-Ray diffraction and Diffuse Reflectance Infrared Fourier Transform Spectroscopy demonstrated the composition of the compounds. Scanning Electron Microscopy and Energy Dispersive X-Ray Spectroscopy determined the compounds were heterogeneous and irregular in shape and size and that the level of silver in the AgGO sample was 57.9 wt.% and the ZnOGO contained 72.65 wt. % zinc. The compounds were tested for their antimicrobial activity against four prominent bacteria; *Escherichia coli*, *Staphylococcus aureus*, *Enterococcus faecium* and *Klebsiella*

26 *pneumoniae*. AgGO was the most effective antimicrobial (Minimum inhibitory concentration
27 *E. coli* / *Enterococcus faecium* 0.125 mg mL⁻¹; *S. aureus* / *K. pneumoniae* 0.25 mg mL⁻¹). The
28 addition of Ag enhanced the activity of GO against the bacteria tested, including the generally
29 recalcitrant *K. pneumoniae* and *Enterococcus faecium*. These findings demonstrated that GO-
30 metal hybrids have the potential to be utilised as novel antimicrobials or biocides in liquid
31 formulations, biomaterials or coatings for use in the treatment of wounds where medically
32 relevant bacteria are becoming increasingly resistant.

33 **Keyword:** Antimicrobials; graphene oxide, biocide; ESKAPE; nano / micro particles;
34 pathogens

35 **1. Introduction**

36 Concerns about bacterial resistance from community-acquired and food-borne pathogens has
37 been growing for a number of years at both national and international levels. Several Gram-
38 positive and Gram-negative bacteria including *Escherichia coli*, *Klebsiella pneumoniae*,
39 *Enterococcus faecium* and *Staphylococcus aureus* are currently considered as emergent global
40 pathogens, which pose a huge global health problem (Boucher et al., 2009).

41 Metals have been used for decades to treat various infectious diseases, and their antimicrobial
42 efficacies are now being re-evaluated owing to the emergence of resilient pathogens. A
43 particular interest has emerged particularly in the use of these compounds for topical /
44 therapeutic use as well as for disinfection to prevent the adhesion and transmission of bacterial
45 species. Silver is one of the most widely investigated metals for antimicrobial applications, and
46 is being used in a number of medical purposes including catheters, biomaterials and wound
47 dressings. Zinc oxide (ZnO) is used in such applications as food packaging (Tayel et al., 2011),
48 textiles (Velmurugan et al., 2016), as antimicrobials (Deokar et al., 2016), and in wound
49 dressings (Chaturvedi et al., 2016). Nanoparticles are interesting in that they can be synthesized
50 with a high surface area to volume ratio and with unusual morphologies that contain sharp

51 edges and corners. Graphite and the graphene derivatives have traditionally been used in
52 electrochemistry, from applications in energy technologies, such as batteries and fuel cells and
53 they have also been used in an array of functional composites (Unwin, et al., 2016). Work has
54 recently suggested that the graphene family of compounds also possess antimicrobial properties
55 (Liu et al., 2011; Wang et al., 2012). By combining the antimicrobial activity of metals together
56 with the physical effect of GO on the bacterial cell walls, it may be hypothesised that the
57 antimicrobial activity of graphene products may be increased.

58 A number of disinfectants and antiseptics have been reported to be showing signs of becoming
59 less effective so there is a need for the development of novel microbicides due to the current
60 limitations (Russel and Chopra, 1990; Jennings et al 2015). Transmission and infection
61 problems due to bacterial adhesion to surfaces can be mitigated in part by the development of
62 alternative antimicrobial sources / biocides. The aim of this work was to determine if metal-
63 GO hybrid compounds demonstrated increased antimicrobial efficacy compared to graphite
64 and GO, against a range of bacteria. The development of such alternative antimicrobial actives
65 may prove beneficial for use in such formulations such as biocidal, disinfecting or topical
66 antimicrobials or cleaning agents or for incorporation into biomaterial coatings.

67 **2. Materials and Methods**

68 *2.1 Synthesis of compounds and characterisation*

69 For the synthesis of the compounds, all chemicals (analytical grade or higher) were used as
70 received from Sigma-Aldrich (UK) without any further purification and all solutions were
71 prepared with deionised water of resistivity not less than 18.2 MΩ cm. Synthetic graphite
72 powder was commercially obtained from Gwent Group (Pontypool, UK).

73 Graphene oxide (GO) was synthesized by the Hummers method *via* the oxidation of synthetic
74 graphite (Hummers Jr and Offeman, 1958). Graphite flakes (5 g) and NaNO₃ (2.5 g) were
75 combined in 115 mL of H₂SO₄ (conc.) and stirred for 30 min. Whilst kept in an ice bath (<5

76 °C), KMnO_4 (15.0 g) was gradually added to the suspension and the rate of addition was
77 controlled to keep the reaction temperature below 15 °C. The mixture was heated to 35 °C for
78 a 30 min period and underwent continuous stirring producing a brown paste. A further dilution
79 was made by adding 250 ml of water to the mixture and the temperature was increased to 70
80 °C for 15 min. The resultant mixture was diluted by adding H_2O until a final volume of 1 L
81 was obtained. Finally, the solution was treated with 15 mL of H_2O_2 (30 % w/w) to terminate
82 the reaction, at which stage the solution became yellow in appearance. For purification, the
83 mixture was filtrated and the obtained solid was washed thoroughly with Milli Q water several
84 times in order to avoid sulphate contamination. After purification, the powder was dried at 60
85 °C during 48 h.

86 In the preparation of the AgGO, a sonochemical reduction method was utilised (Anandan and
87 Muthukumaran, 2015). Following preparation of the GO, 0.5 g was added to 150 mL of
88 ethylene glycol and sonicated for 30 min. In a separate vesicle, 1.0 g of silver nitrate was added
89 to 20 mL of ethylene glycol and sonicated for 30 min. The silver nitrate dispersion was added
90 drop-wise to the GO solution whilst undergoing sonication for 30 min to produce a
91 homogeneous mixture. Finally, 50 mL of 0.1 M NaBH_4 was added to the resultant AgGO
92 mixture and a further 30 min of sonication was performed. The product was purified with
93 repeated steps of H_2O and ethanol washing, after which the solution was dried at 50 °C.

94 The ZnOGO was fabricated by dissolving 5.0 g GO in 200 mL of N, N,-dimethylformamide
95 (DMF), along with 20 ml of 1 M zinc acetate dihydrate (pH of 6.5). The homogeneous solution
96 was heated to 60 °C and was stirred continuously for 120 min, after which the solution was
97 heated to 250 °C. Following solvent evaporation, partial ZnO / ZnOHGO was produced. The
98 resulting dried product was collected and ground in an agate mortar prior to being annealed at
99 450 °C for 120 min within atmospheric conditions to obtain the final ZnOGO product (Liu et
100 al., 2012).

101 *2.1.1 Preparation of compounds for testing*

102 For the analysis of the fabricated compounds, 20 mg of each test compound was added to 20
103 mL of sterile distilled water. The samples were vortexed for 10 s and immediately 10 μ L of
104 prepared sample was pipetted onto a 10 mm x 10 mm polished silicon wafer (Montco Silicon
105 Technologies, USA) and air dried for 30 min. The samples were stored at room temperature,
106 in desiccators until use.

107 *2.1.2 X-Ray Diffraction (XRD)*

108 In order to identify the crystal phase of the compounds, X-Ray Diffraction (XRD) was
109 performed using a PANalytical X'pert powder diffraction platform. Nickel filtered copper K_{α}
110 radiation ($\lambda = 1.54 \text{ \AA}$) was used, with an anode voltage of 40 kV an anode current of 30 mA. A
111 reflection transmission spinner stage (15 rpm) was implemented to hold the powder samples.
112 The XRD parameters were step size: 0.13; sample: powder; slit (antiscatter) size: $1/4^{\circ}$. The 2θ
113 range was set between 10° and 100° , in correspondence with literature ranges associated with
114 the characterised samples (Li et al., 2007; Zhou et al., 2007; Kumar et al., 2013; Chowdhuri et
115 al., 2015; Liu et al., 2016). Additionally, to ensure well-defined peaks, an exposure of 50 s per
116 2θ step was implemented.

117 *2.1.3 Diffuse Reflectance Infrared Fourier Transform Spectroscopy (DRIFTS)*

118 Diffuse Reflectance Fourier Transform Infrared Spectroscopy (DRIFTS) was carried out using
119 a Spectra-Tech DRIFTS cell fitted in a Thermo – Nicolet Nexus FTIR spectrophotometer. The
120 instrument was thoroughly purged (30 L / min) with CO_2 and water-free air, produced using a
121 Balaston purge gas generator. All samples were diluted to ca. 5 % wt. in finely ground KBr
122 (Sigma, UK). The samples were used as received, with no further grinding. The sample was
123 folded into the pre-ground KBr using a micro-spatula. The micro-sampling cup was over-filled
124 slightly and the cup dropped from a height of 1 cm onto the bench in order to shake off the
125 excess mixture whilst at the same time, produce a slightly domed and naturally randomised,

126 surface of KBr diluted sample. The same batch of ground KBr was used as the background.
127 The background and sample spectra were made up of 164 scans with resolution set to 4 cm⁻¹.
128 As the sample was diluted with KBr there were no specular reflection components so a blocker
129 was not used. Spectra were plotted in absorbance (Liauw, 2003).

130 *2.1.4 Scanning Electron Microscopy (SEM) and Energy Dispersive X-Ray Spectroscopy (EDX)*

131 In order to determine the shape, size and atomic elemental weight of the compounds, the
132 samples were fixed to stubs using carbon tabs (Agar, UK). Scanning Electron Microscopy (Carl
133 Zeiss Ltd.) was carried out using a Supra 40VP SEM with SmartSEM software. Energy
134 Dispersive X-Ray (EDAX Inc.) was carried out using an Apollo 40 SDD system with Genesis
135 software.

136 **2.2 Microbiology and antibacterial testing**

137 *2.2.1 Stock cultures of bacteria*

138 In preparation for the antimicrobial assays, stock cultures of *S. aureus* NCTC 4137, *K.*
139 *pneumoniae* NCTC 9633 or *E. coli* NCTC 10418 were inoculated onto nutrient agar (NA) or
140 nutrient broth (NB) and incubated at 37 °C for 24 h. Stock cultures of *Enterococcus faecium*
141 NCTC 7171 were cultured onto Columbia blood agar with horse blood in a 5 %, Brain heart
142 infusion agar (BHIA) (Oxoid, UK) or brain heart infusion broth (BIHB) and incubated in 5 %
143 CO₂ for 24 h at 37 °C. All medias were obtained from Oxoid (UK).

144 *2.2.2 Preparation of microbiological cultures*

145 Ten millilitres of appropriate broth was inoculated with a single colony of bacteria and
146 incubated overnight according to the above conditions. Following incubation, cells were
147 harvested at 567 × g for 10 min and washed once, re-suspended in sterile distilled water,
148 vortexed for 30 s, and then centrifuged again at 567 × g for 10 min. The inocula were examined
149 in a spectrophotometer at 540 nm and compared against a blank of sterile distilled water to
150 determine their optical density. They were then diluted accordingly and quantified using serial

151 dilutions. The cell concentrations corresponded to; *E. coli* 4.20×10^8 , *S. aureus* 1.30×10^8 ,
152 *Enterococcus faecium* 3.95×10^8 and *K. pneumoniae* 2.82×10^8 colony forming units per mL
153 (CFU / mL).

154 *2.2.3 Zones of inhibition*

155 The zones of inhibition assays were performed to test the antimicrobial efficacy of each
156 individual compound (n = 24). One hundred microliters of prepared cell suspension was
157 pipetted and spread across the surface of the agar. Three equal wells (8 mm diameter) were cut
158 out of the each agar plates. To each of the wells, 100 μ L of suspended compound was added.
159 The plates were incubated in the appropriate air conditions and temperature for 24 h. Following
160 incubation, the zones of inhibition was measured in mm from four sides of each well to
161 determine an average mean value (n = 24).

162 *2.2.4 Minimum inhibitory concentrations (MIC)*

163 The minimal inhibitory concentration (MIC) is defined as the lowest concentration of
164 antimicrobial to prevent bacterial growth (Russel and Chopra, 1990). One millilitre of triphenyl
165 tetrazolium chloride (TTC) blue metabolic dye (Sigma-Aldrich, UK), was added into 9 mL of
166 the cell suspension so that the working concentration of the dye was 0.15 % w/v. To determine
167 the MIC, the samples and bacteria were added to a 96 well flat-bottomed microtiter plate (MTP)
168 and a serial dilution method used across the plate. A bacterial suspension without any
169 compound (positive control) and un-inoculated broth (negative control) was included. After
170 incubation, the MIC was taken as lowest concentration that inhibited the visible growth of the
171 bacteria by comparison with the controls. Growth was indicated by a change of colour in the
172 well to dark blue / purple.

173 *2.3.5 Minimum Bactericidal Concentration (MBC)*

174 The MBC is defined as the lowest concentration required to completely inactivate the inoculum
175 at a given time (Humphreys et al., 2011). To perform the MBC assays, 25 μ L was sampled and

176 pipetted onto agar plates from the MIC well that showed no growth and also from the first well
177 that showed growth and incubated overnight in appropriate conditions. After incubation, the
178 lowest concentration well sample that showed no growth on the agar plate was determined to
179 be the MBC for that test sample.

180 *2.3.6 Statistical analysis*

181 Statistical tests were carried out using a two tailed distribution *t*-test with two sample
182 homoscedastic variance. Results were reported as mean \pm standard error or percentage and any
183 observed differences were considered significant at a $p < 0.05$.

184 **3. Results**

185 *3.1 Particle characterisation*

186 In order to assess the antibacterial activity of four compounds, graphite, GO, AgGO and
187 ZnOGO, the compounds and hybrid molecules were firstly obtained or synthesized, then
188 characterised and then tested using well-established antibacterial assays. The XRD patterns
189 relating to the graphite powder produced the expected characteristic diffraction peaks at $2\theta =$
190 26.6° , 44.7° and 54.6° , corresponding to the (002), (101) and (004) diffraction peaks of graphite
191 powder respectively (Fig. 1a and a'). XRD (Fig.1 a') plotted over a narrower 2θ range and with
192 a finer counts scale, showed some disordered material as evidenced by the wide peak between
193 ca. 7° and 17° and by a characteristic 'sharp' peak was evident at $2\theta = 11.8^\circ$ (Fig. 1b). The
194 composition of the GO sample was confirmed as corresponding to the (002) diffraction peak
195 of disordered GO. Application of the Bragg equation to the reflection peak angles, revealed
196 that the interplanar distance increased from 0.35 nm in graphite to 0.75 nm in graphene oxide.
197 For the latter, EDX gave 54.6 wt.% C and 45.3 wt.% O (O/C ratio = 0.83), whilst the former
198 (graphite) had an oxygen content of only 8.9 wt.%, with all of the remainder being carbon
199 (Table 1).

200 The ZnOGO was confirmed by XRD to have a high concentration of ZnO (Fig. 1c). Diffraction
201 peaks were evident at $2\theta = 32.2^\circ, 34.8^\circ, 36.7^\circ, 48.0^\circ, 57.0^\circ, 63.3^\circ, 66.8^\circ, 69.5^\circ$ and 72.9° which
202 corresponded to the (100), (002), (101), (102), (110), (103), (112), (201) and (004) crystalline
203 planes of ZnO, respectively (Liu et al., 2012). EDX revealed that the ZnOGO contained C (8.60
204 wt.%), O (18.75 wt.%) and Zn (72.65 wt.%). Due to the low level of carbon in ZnOGO, the
205 (002) reflection for GO (centred at ca. 10°) (Fig. 1c') was very weak. The ZnOGO was light
206 grey in colour thus confirming the presence of carbon in the sample.

207 Following analysis of the AgGO, the diffraction peaks occurred at $2\theta = 38.7^\circ, 44.9^\circ, 65.0^\circ$ and
208 77.9° (Fig. 1d). These peaks corresponded to the (111), (200), (220) and (311) crystallographic
209 planes of face-centred cubic silver. A small amount of Ag_2O was present as evidenced by the
210 corresponding (110) and (111) reflections at 28.4° and 33.8° respectively. The (002)
211 reflection of the GO was significantly attenuated (Fig. 1d) and shifted from 11.8° to 10° ($d_{(002)}$
212 $= 0.86$ nm). There was also a broad reflection peak over the range 12° and 18° , with two small
213 peaks centred at 15° and 20° (Fig. 1d') whereby corresponding d values were 0.60 nm and 0.44
214 nm, respectively, indicating the presence of disordered structures.

215 Diffuse Reflectance Infrared Fourier Transform Spectroscopy (DRIFTS) was used to further
216 characterise the compounds. Overlaid DRIFTS spectra of the $4000\text{ cm}^{-1} - 2000\text{ cm}^{-1}$ region for
217 the graphite, GO and AgGO demonstrated that the DRIFTS spectrum of graphite (Fig. 2a) was
218 largely featureless as expected, though there was a small and negative hydrogen bonded OH
219 stretching peak which was due to there being slightly more moisture in the background than
220 the sample. The size and position of this band did not hinder interpretation of this spectral
221 region for GO or AgGO. Graphene oxide (Fig. 2b) showed the expected broad envelope of
222 hydrogen bonded OH stretching vibrations from 3700 cm^{-1} to 2500 cm^{-1} , together with some
223 OH bands at 3650 cm^{-1} that appeared to be much less involved in hydrogen bonding. Interaction
224 of the GO with the silver (Fig. 2c) appeared to remove the latter OH stretching band and

225 generally attenuated the hydrogen bonded OH stretching within the region above 3350 cm^{-1} .
226 There were some small aliphatic C-H stretching vibrations at 2946 cm^{-1} (asymmetric) and 2877
227 cm^{-1} (symmetric). The 2000 cm^{-1} to 400 cm^{-1} region of the same three samples demonstrated
228 that the graphite spectrum (Fig. 3a) was again featureless apart from a small negative peak at
229 1650 cm^{-1} which could be assigned to an O-H bend of water, indicating again that there was
230 slightly more moisture in the background than the sample; this peak did not interfere with
231 interpretation. The GO featured all the expected peaks (Fig. 3b); carbonyl stretching (1738 cm^{-1});
232 skeletal aromatic C=C vibrations (1615 cm^{-1}); C-OH stretching (1356 cm^{-1}); C-O-C
233 stretching (1225 cm^{-1}); C-O stretching (1056 cm^{-1}); aromatic C-H bending (849 cm^{-1}). The
234 AgGO (Fig. 3c) also featured the same absorption bands but with the following significant
235 differences: carbonyl stretching, skeletal aromatic C=C vibrations and C-O-C stretching
236 vibrations were all red-shifted by 10 cm^{-1} , 29 cm^{-1} and 5 cm^{-1} , respectively. Furthermore, the
237 C-O vibration was split and consisted of a blue shifted component (1078 cm^{-1}) and a red shifted
238 component (1037 cm^{-1}) (Table 2).

239 Overlaid spectra of the synthesised ZnO and ZnOGO demonstrated in both spectra, carbon
240 dioxide absorption at 2350 cm^{-1} (Fig. 4) and carbonate absorptions at ca. 1580 cm^{-1} and 1380
241 cm^{-1} (Fig. 5). SEM showed that the compounds were heterogeneous and irregular in size (Table
242 3) and shape (Fig. 6). Graphite (Fig. 6a) had a flattened, irregular, random orientation,
243 fractured, sheet like morphology with sharp, cleaved edges (0.10 μm – 25.7 μm). Graphene
244 oxide (Fig. 6b) was composed of aggregated creased platelets (0.20 μm – 20.0 μm). The
245 ZnOGO (Fig. 6c) consisted of numerous aggregated nanoparticles and / or nanoparticles
246 covering micron-sized particles (0.05 μm – 30.0 μm). AgGO (Fig. 6d) was similar to GO in
247 appearance; creased aggregated platelets with a random scattering of nanoparticles (possibly
248 silver and / or silver oxide) (0.01 μm - 13.0 μm).

249 *3.2 Microbiological analysis*

250 Zones of inhibition assays were carried out against Gram-negative *E. coli* and *K. pneumoniae*
251 and Gram-positive *S. aureus* and *Enterococcus faecium* (Fig. 7). Following the zone of
252 inhibition assays, all the compounds demonstrated antimicrobial activity against *E. coli* and all
253 the GO-containing compounds demonstrated antimicrobial activity against *S. aureus*. Graphite
254 was only effective against *E. coli* and thus demonstrated a significantly greater antimicrobial
255 efficacy than GO or ZnOGO against this bacteria ($p > 0.05$). The most effective antimicrobial
256 overall against the bacteria using zones of inhibition was AgGO which provided the greatest
257 zones of inhibition against *E. coli* (4.48 mm) and *S. aureus* (4.50 mm).

258 The MIC results demonstrated that against *E. coli* all the compounds were effective at
259 concentrations of 0.125 mg mL⁻¹. Against *S. aureus*, graphene oxide was the most effective
260 (0.125 mg mL⁻¹) whilst AgGO was the most effective against *Enterococcus faecium* (0.125 mg
261 mL⁻¹). *K. pneumoniae* was again the most difficult bacteria to inhibit. However, the ZnOGO
262 and AgGO compounds demonstrated statistically significant inhibitory effects compared to the
263 graphite and GO compounds against *K. pneumoniae* at concentrations of 0.25 mg mL⁻¹ ($p >$
264 0.05). MBCs demonstrated that against *E. coli*, ZnOGO and AgGO were the most effective at
265 0.125 mg mL⁻¹. GO, ZnOGO and AgGO were all effective against *S. aureus* at a concentration
266 of 0.25 mg mL⁻¹ whilst AgGO was the most effective against *Enterococcus faecium* (0.125 mg
267 mL⁻¹) (Fig. 8b). It was demonstrated that as with the other assays, *K. pneumoniae* was the most
268 difficult bacteria to eradicate, demonstrating the greatest MBC values. However, AgGO was
269 the most effective hybrid compound against this bacteria at a concentration of 0.25 mg mL⁻¹.

270 **4. Discussion**

271 *4.1 Characterisation of compounds*

272 The XRD patterns relating to the graphite powder produced the expected characteristic
273 diffraction peaks (Peng et al., 2013). The composition of the GO sample was confirmed
274 (Chowdhuri et al., 2015) and it was evident that the (002) reflection had shifted to a lower

275 angle and was of much lower intensity, relative to the same reflection in graphite. These
276 observations are well established and indicate the formation of pendent oxygen containing
277 functional groups on the top and bottom surfaces of the basal planes that increase the
278 interplanar distance; this resulted in the shift of the (002) reflection to a lower angle
279 demonstrating significantly decreased stacking uniformity (resulting in reduced reflection
280 intensity). This is consistent with the DRIFTS data that indicated prolific functionalisation. The
281 XRD also demonstrated disruption of the relatively ordered stacking of GO platelets due to
282 non-uniform intercalation by the ZnO nanoparticles and / or coverage of the ZnO particles by
283 GO, which may have contributed to a reduced intensity of the reflection (Chowdhuri et al.,
284 2015). The AgGO peaks corresponded to crystallographic planes of face-centred cubic silver
285 (Zhou et al., 2007). A small amount of Ag₂O was present but as the atomic radius of silver is
286 0.17 nm, it is conceivable that individual silver atoms may have intercalated the platelets
287 (Dhoondia and Chakraborty, 2012). The attenuation of the (002) reflection indicated that the
288 otherwise relatively regular stacking of GO had probably been disrupted by non-uniformly
289 sized Ag nanoparticles between the GO platelets. It is also plausible that the GO may form a
290 coating on the Ag nanoparticles (Oo, 2007; Das et al., 2011; Ma et al., 2011). The level of
291 silver (by EDX) in the sample was 57.9 wt.%; a mix of GO intercalation by Ag nanoparticles
292 and GO coating of Ag nanoparticles may therefore be likely. The level of carbon (20.3 wt.%)
293 can be accommodated by the proposed structures of the hybrid. The oxygen in the Ag₂O will
294 have contributed to the amount of overall oxygen identified in the sample (21.8 wt %).

295 The DRIFTS spectrum of graphite was largely featureless as expected. GO showed the
296 expected broad envelope of hydrogen bonded OH stretching vibrations. AgGO appeared to
297 remove the latter OH stretching band and generally attenuated the hydrogen bonded OH
298 stretching. This may be due to the interaction of the silver with weakly hydrogen bonded OH
299 groups (phenolic OH and other OH) of the GO. The more general attenuation of the hydrogen

300 bonded O-H bands, within the region above 3350 cm^{-1} , may be related to reduced water content
301 in the AgGO and / or interaction of the silver with the hydrogen bonded OH groups of the GO.
302 There were some small aliphatic C-H stretching vibrations. These may be due to residual
303 ethylene glycol from the compound synthesis and to a lesser extent, residual ethanol from
304 washing. The C-O vibration was split and consisted of a blue shifted component (1078 cm^{-1})
305 and a red shifted component (1037 cm^{-1}). These observations indicated a significant interaction
306 of the GO platelets with the silver. The latter is further supported by a blue shift in the aromatic
307 C-H bending and C-OH stretching band. Interaction of the silver with carbonyl species and
308 with the residual *p*-electrons in the GO would lead to the observed red shifts as the bond
309 vibration was damped by interaction with the electron orbitals of silver atoms. This would also
310 result in shortening of the aromatic C-H bonds and phenolic and carboxylic acid C-OH bonds,
311 hence giving rise to the observed blue shift. The split in the C-O vibration indicated silver
312 interactions having varying effects on the different ether linkages in the GO. It may be
313 speculated that the ether groups at the platelet edges would be blue shifted and those actually
314 pendant from a platelet surface may be red-shifted due to their interaction with the silver atoms.
315 These observations are supported by the XRD data which indicated that the usual relatively
316 ordered structure of the GO had been destroyed by its interaction with the silver. It may be that
317 the silver atoms / particles had intercalated the layers resulting in highly non-uniform stacking.
318 This would lead to the significantly attenuated and broadened GO related reflections in the
319 XRD data for the AgGO.

320 The features observed using the DRIFTS analysis were expected in the ZnO that had been
321 synthesised via this route since the carbonate and carbon dioxide would be decomposition
322 products of the starting materials (Selim et al., 2015). The carbonate would have been
323 converted to CO_2 as the annealing temperature increased, resulting in the CO_2 becoming
324 trapped within the structure. Interestingly, the OH stretching bands were more intense in the

325 ZnOGO, and it may be that these were related to the GO, though the associated carbonyl and
326 C-O bands could not be resolved. This may be explained by the strong association between the
327 GO and ZnO resulting in attenuation of these vibrations. The GO may have coated the surface
328 of the synthesised ZnO particles and / or could have become interleaved within the synthesised
329 ZnO structures. In either case, the relatively ordered stacking of the GO platelets had become
330 disrupted. The XRD data supports the latter proposition. The other area of interest in these
331 spectra was the Zn-O bending vibrations at ca. 440 and 520 cm^{-1} . In the ZnOGO, the ZnO band
332 at 520 cm^{-1} was stronger than in the synthesised ZnO (Fig. 5b). To the authors knowledge, such
333 observations have not been reported elsewhere, but it may be related to a difference in the
334 chemical environment and possibly due to the interactions with the GO.

335 SEM demonstrated that the compounds were heterogeneous and irregular in size and shape.
336 The ZnOGO particles had the greatest size range (0.05 μm – 30 μm), whereas AgGO and
337 ZnOGO had the smallest sized particles (0.01 μm and 0.05 μm respectively) demonstrating the
338 availability of both nano- and micron sized particles.

339 *4.2 Microbiology*

340 The zone of inhibition assays demonstrated that none of the compounds had any effect against
341 *Enterococcus faecium* or *K. pneumoniae*. This may be due to the zone of inhibition method
342 being carried out using a semi-solid media; this combined with the thick capsule of the *K.*
343 *pneumoniae* and the insusceptible nature of the *Enterococcus faecium* may have resulted in the
344 reduced antimicrobial effect demonstrated. Further, the bacteria in this method were growing
345 on the agar in colonies. These ‘communities’ of bacteria may have been more resistant to the
346 antimicrobial effects of the compounds, similar to the effects observed when bacteria form
347 biofilms (Gilbert et al., 2002) rather than what was observed when the bacteria are in planktonic
348 form as in the MIC and MBC.

349 Work by others has demonstrated the antibacterial activities of graphite and graphite oxide
350 towards *E. coli* and it was found that a GO dispersion demonstrated an 89.7% of loss viability
351 at 40 mg mL⁻¹ (Liu et al., 2007). In our work, we demonstrated an antimicrobial activity of GO
352 at much lower concentrations against the four bacterial strains tested (MIC = 0.125 mg mL⁻¹ –
353 0.5 mg mL⁻¹; MBC = 0.25 mg mL⁻¹ – 0.5 mg mL⁻¹). Work by Xie et al. (2011) demonstrated
354 the MIC of ZnO nanoparticles for *Escherichia coli* O157:H7 was found to be 0.4 mg mL⁻¹. In
355 comparison with our work, ZnOGO was the most antimicrobial compound against *E. coli* with
356 an MIC at the lower concentration of 0.125 mg mL⁻¹. However, the *E. coli* used in our study
357 was a different strain. The ZnOGO was also inhibitory against *S. aureus*, *Enterococcus faecium*
358 and *K. pneumoniae* at a MIC of 0.25 mg mL⁻¹. GO and AgGO were also effective against *S.*
359 *aureus* and *Enterococcus faecium* at concentrations of 0.125 mg mL⁻¹. Work by others also
360 demonstrated that the MIC for ZnO nanoparticles was 1.5 mg mL⁻¹ and 3.1 mg mL⁻¹ against *S.*
361 *aureus* and *E. coli* respectively demonstrating that in some cases our ZnOGO compound was
362 more effective than the antimicrobial action of ZnO alone used in other studies (Franklin et al.,
363 2007; Azam et al., 2012). The MIC against *Enterococcus faecium* and *K. pneumoniae* was
364 optimal with the AgGO hybrid compound. ZnOGO also demonstrated the same MIC as AgGO
365 against *K. pneumoniae*.

366 Results from the MBC assays demonstrated that *K. pneumonia* was the most difficult bacteria
367 to eradicate. Work by others using MBC assays with 18 nm nanoparticles of ZnO demonstrated
368 that the concentration of particles required against *E. coli* was 0.018 mg mL⁻¹ and 0.016 mg
369 mL⁻¹ against *S. aureus* (Xie et al., 2011). However, in contrast with their results, our compounds
370 required greater concentrations in order to obtain the MBC. This may be explained by the
371 particle size of our compounds being generally larger. It has been suggested that the smaller
372 the size of the compounds, the greater the antimicrobial activity of the agent, however

373 contradictory results have been reported where size dependent effects were not found to
374 influence the antimicrobial activity of ZnO (Chen et al., 2014).

375 The antimicrobial activity of the hybrid compounds may be explained in part by either the
376 shape of the compound particles or by the percent of active facets. The atomic structure of the
377 particle surface will affect its interaction with the bacterial cells (Selim et al., 2015). It is
378 expected that the adsorption of atoms and molecules as a result of the interaction of the particles
379 with the environment will be altered on the different planes, thus the difference in the atomic
380 structure of the particles may result in a difference in their surface properties that could affect
381 their interaction with the bacteria, leading to different antimicrobial efficacies (Pal et al., 2007).
382 It has been suggested that high density facets with (111) faces exhibit greater amounts of
383 antimicrobial activity (Pal et al., 2007). This is in agreement with our work since the AgGO
384 demonstrated the greatest numbers of (111) planes. Combined with the shape of the
385 compounds, these crystal structures can influence their mechanism of bacterial internalisation
386 of the cell wall (Sirelkhatim et al., 2015).

387 Work by Liu et al. (2011) focused on the interactions of GO and graphite on bacterial
388 membranes against *Escherichia coli*. In agreement with our results, they showed that a GO
389 dispersion had a greater amount on antibacterial activity than graphite. GO and graphite are
390 thought to confer antimicrobial activity due to membrane stress on the bacterial cells induced
391 by the sharp edges of the compounds (Liu et al., 2011; Chen et al., 2014). An interesting fact
392 that was evidenced in this work was that the type of antimicrobial assay used produced a range
393 of results and thus it may be concluded that the use of one antimicrobial assay to determine the
394 efficacy of compounds is not sufficient. Further, the type of antimicrobial assay used should be
395 selected in line with the proposed final application of the antimicrobials.

396 Following each of the antimicrobial tests, AgGO demonstrated the greatest overall
397 antimicrobial efficacies. *E. coli* was the most susceptible to the compounds followed by *S.*

398 *aureus*, *Enterococcus faecium* and finally *K. pneumoniae*. This can be explained in part by the
399 nature of the microorganisms physiology. The Gram-negative microorganisms *E. coli* and *K.*
400 *pneumoniae* are surrounded by an outer and inner cell membrane which have between them a
401 thin layer of peptidoglycan. However, *K. pneumoniae* also has a large polysaccharide capsule
402 surrounding the bacterial cell; in addition, this capsule acts as a barrier to antimicrobial agents
403 (Highsmith and Jarvis, 1985). *S. aureus* and *Enterococcus faecium* are Gram-positive bacteria
404 that have a cell membrane, chiefly composed of thick peptidoglycan. However, Enterococci
405 are intrinsically more resistant to many antibiotics since unlike acquired resistance and
406 virulence traits which are usually encoded by plasmids or transposon elements, their intrinsic
407 resistance is based on chromosomal genes (Huycke et al., 1998). Further, a number of
408 antibiotics demonstrate bacteriostatic but not bactericidal activity against *Enterococcus*
409 *faecium* bacteria (Huycke et al., 1998). Thus, the use of AgGO against these two resilient
410 bacteria may be an important step in maintaining the hygienic status of areas into which the
411 molecule is applied or incorporated.

412 **5. Conclusions**

413 ZnOGO and AgGO hybrid compounds were successfully produced and characterised. AgGO
414 was the most effective antimicrobial and enhanced the activity of GO. The effect of the
415 compounds on the bacteria did not relate to the Gram-positive or Gram-negative structures of
416 the bacteria but rather, was due to their microorganisms overall physiology. GO-metal hybrids
417 have the potential to be beneficially utilised as novel antimicrobials or biocides in settings
418 where bacteria are becoming increasingly problematic.

419 **Acknowledgements**

420 The authors would like to acknowledge that the work was funded by Manchester Metropolitan
421 University. P. Ramalingam would also like to acknowledge a Newton-Bhabha fellowship from
422 the British Council.

423 **References**

424 Anandan, S., Muthukumar, S., 2015. Microstructural, crystallographic and optical
425 characterizations of Cu-doped ZnO nanoparticles co-doped with Ni. *Journal of Materials*
426 *Science: Materials in Electronics* 26, 4298-4307.

427 Azam, A., Ahmed, A. S., Oves, M., Khan, M. S., Habib, S. S., Memic, A., 2012. Antimicrobial
428 activity of metal oxide nanoparticles against Gram-positive and Gram-negative bacteria: A
429 comparative study. *International Journal of Nanomedicine* 7, 6003-6009.

430 Boucher, H. W., Talbot, G. H., Bradley, J. S., Edwards, J. E., Gilbert, D., Rice, L. B., Scheld,
431 M., Spellberg, B., Bartlett, J., 2009. Bad Bugs, No Drugs: No ESKAPE! An Update from the
432 Infectious Diseases Society of America. *Clinical Infectious Diseases* 48, 1-12.

433 Chaturvedi, A., Bajpai, A.K., Bajpai, J., Singh, S.K., 2016. Evaluation of poly (vinyl alcohol)
434 based cryogel-zinc oxide nanocomposites for possible applications as wound dressing
435 materials. *Materials Science & Engineering C-Materials for Biological Applications* 65, 408-
436 418.

437 Chen, J., Peng, H., Wang, X., Shao, F., Yuan, Z., Han, H., 2014. Graphene oxide exhibits
438 broad-spectrum antimicrobial activity against bacterial phytopathogens and fungal conidia by
439 intertwining and membrane perturbation. *Nanoscale* 6, 1879-1889.

440 Chowdhuri, A. R., Tripathy, S., Chandra, S., Roy, S., Sahu, S. K., 2015. A ZnO decorated
441 chitosan-graphene oxide nanocomposite shows significantly enhanced antimicrobial activity
442 with ROS generation. *RSC Advances* 5, 49420-49428.

443 Das, M. R., Sarma, R. K., Saikia, R., Kale, V. S., Shelke, M. V., Sengupta, P., 2011. Synthesis
444 of silver nanoparticles in an aqueous suspension of graphene oxide sheets and its antimicrobial
445 activity. *Colloids and Surfaces B: Biointerfaces* 83, 16-22.

446 Deokar, A.R., Shalom, Y., Perelshtein, I., Perkas, N., Gedanken, A., Banin, E., 2016. A
447 topical antibacterial ointment made of Zn-doped copper oxide nanocomposite. *Journal of*
448 *Nanoparticle Research* 18, 1-6.

449 Dhoondia, Z. H., Chakraborty, H., 2012. Lactobacillus Mediated Synthesis of Silver Oxide
450 Nanoparticles. *Nanomaterials and Nanotechnology* 2, 15.

451 Franklin, N. M., Rogers, N. J., Apte, S. C., Batley, G. E., Gadd, G. E., Casey, P. S., 2007.
452 Comparative toxicity of nanoparticulate ZnO, bulk ZnO, and ZnCl₂ to a freshwater microalga
453 (*Pseudokirchneriella subcapitata*): the importance of particle solubility. *Environmental Science*
454 *and Technology* 41, 8484-8490.

455 Gilbert, P., Allison, D. G., McBain, A. J., 2002. Biofilms in vitro and in vivo: do singular
456 mechanisms imply cross-resistance? *Journal of Applied Microbiology* 92, 98s-110s.

457 Highsmith, A. K., Jarvis, W. R., 1985. *Klebsiella pneumoniae*: selected virulence factors that
458 contribute to pathogenicity. *Infection Control* 6, 75-77.

459 Hummers Jr, W. S., Offeman, R. E., 1958. Preparation of graphitic oxide. *Journal of the*
460 *American Chemical Society* 80, 1339-1339.

461 Humphreys, G., Lee, G. L., Percival, S. L., McBain, A. J., 2011. Combinatorial activities of
462 ionic silver and sodium hexametaphosphate against microorganisms associated with chronic
463 wounds. *Journal of Antimicrobial Chemotherapy* 66, 2556-2561.

464 Huycke, M. M., Sahm, D. F., Gilmore, M. S., 1998. Multiple-drug resistant enterococci: the
465 nature of the problem and an agenda for the future. *Emerging Infectious Diseases* 4, 239-249.

466 Jennings, M. C., Minbiole, K. P., Wuest, W. M., 2015. Quaternary Ammonium Compounds:
467 An Antimicrobial Mainstay and Platform for Innovation to Address Bacterial Resistance. *ACS*
468 *Infectious Diseases* 1, 288-303.

469 Kumar, S. S., Venkateswarlu, P., Rao, V. R., Rao, G. N., 2013. Synthesis, characterization and
470 optical properties of zinc oxide nanoparticles. *International Nano Letters* 3, 30.

471 Li, Z. Q., Lu, C. J., Xia, Z. P., Zhou, Y., Luo, Z., 2007. X-ray diffraction patterns of graphite
472 and turbostratic carbon. *Carbon* 45, 1686-1695.

473 Liauw, C. M., 2003. *Particulate Filled Composites (2nd Edition)*, Ed. Rotheron RN, Smithers
474 RAPRA technology.

475 Liu, H., Zhang, Y., Yang, H., Xiao, W., Sun, L., 2016. Filter Paper Inspired Zinc Oxide
476 Nanomaterials with High Photocatalytic Activity for Degradation of Methylene Orange.
477 *Journal of Chemistry* 2016, 1-7.

478 Liu, L. F., Barford, J., Yeung, K. L., Si, G., 2007. Non-UV based germicidal activity of metal-
479 doped TiO₂ coating on solid surfaces. *Journal of Environmental Science (China)* 19, 745-750.

480 Liu, Q., Yao, X., Zhou, X., Qin, Z., Liu, Z., 2012. Varistor effect in Ag-graphene/epoxy resin
481 nanocomposites. *Scripta Materialia* 66, 113-116.

482 Liu, S., Zeng, T. H., Hofmann, M., Burcombe, E., Wei, J., Jiang, R., Kong, J., Chen, Y., 2011.
483 Antibacterial activity of graphite, graphite oxide, graphene oxide, and reduced graphene oxide:
484 membrane and oxidative stress. *ACS Nano*. 5, 6971-6980.

485 Ma, J., Zhang, J., Xiong, Z., Yong, Y., Zhao, X. S., 2011. Preparation, characterization and
486 antibacterial properties of silver-modified graphene oxide. *Journal of Materials Chemistry* 21,
487 3350-3352.

488 Oo, H. W. M., 2007. *Infrared Spectroscopy of Zinc Oxide and Magnesium Nanostructures*.
489 Ph.D Thesis. Washington State University.

490 Pal, S., Tak, Y. K., Song, J. M., 2007. Does the Antibacterial Activity of Silver Nanoparticles
491 Depend on the Shape of the Nanoparticle? A Study of the Gram-Negative Bacterium
492 *Escherichia coli*. *Applied and Environmental Microbiology* 73, 1712-1720.

493 Peng, S. G., Fan, X. J., Li, S., Zhang, J., 2013. Green synthesis and characterization of graphite
494 oxide by orthogonal experiment. *Journal of the Chilean Chemical Society* 58, 2213-2217.

495 Russel, A. D., Chopra, I., 1990. Understanding antimicrobial resistance and action. Ellis
496 Horwood, Chichester.

497 Selim, M. S., El-Safty, S. A., El-Sockary, M. A., Hashem, A. I., Abo Elenien, O. M., El-Saeed,
498 A. M., Fatthallah, N. A., 2015. Modeling of spherical silver nanoparticles in silicone-based
499 nanocomposites for marine antifouling. *RSC Advances* 5, 63175-63185.

500 Sirelkhatim, A., Mahmud, S., Seeni, A., Kaus, N. H. M., Ann, L. C., Bakhori, S. K. M., Hasan,
501 H., Mohamad, D., 2015. Review on Zinc Oxide Nanoparticles: Antibacterial Activity and
502 Toxicity Mechanism. *Nano-Micro Letters* 7, 219-242.

503 Tayel, A. A., El-Tras, W. F., Moussa, S., El-Baz, A. F., Mahrous, H., Salem, M. F., Brimer,
504 L., 2011. Antibacterial action of zinc oxide nanoparticles against foodborne pathogens. *Journal*
505 *of Food Safety* 31, 211-218.

506 Velmurugan, P., Park, J.H., Lee, S.M., Yi, Y.J., Cho, M., Jang, J.S., Myung, H., Bang, K.S.,
507 Oh, B.T., 2016. Eco-friendly approach towards green synthesis of zinc oxide nanocrystals
508 and its potential applications. *Artificial Cells Nanomedicine and Biotechnology* 44, 1537-
509 1543.

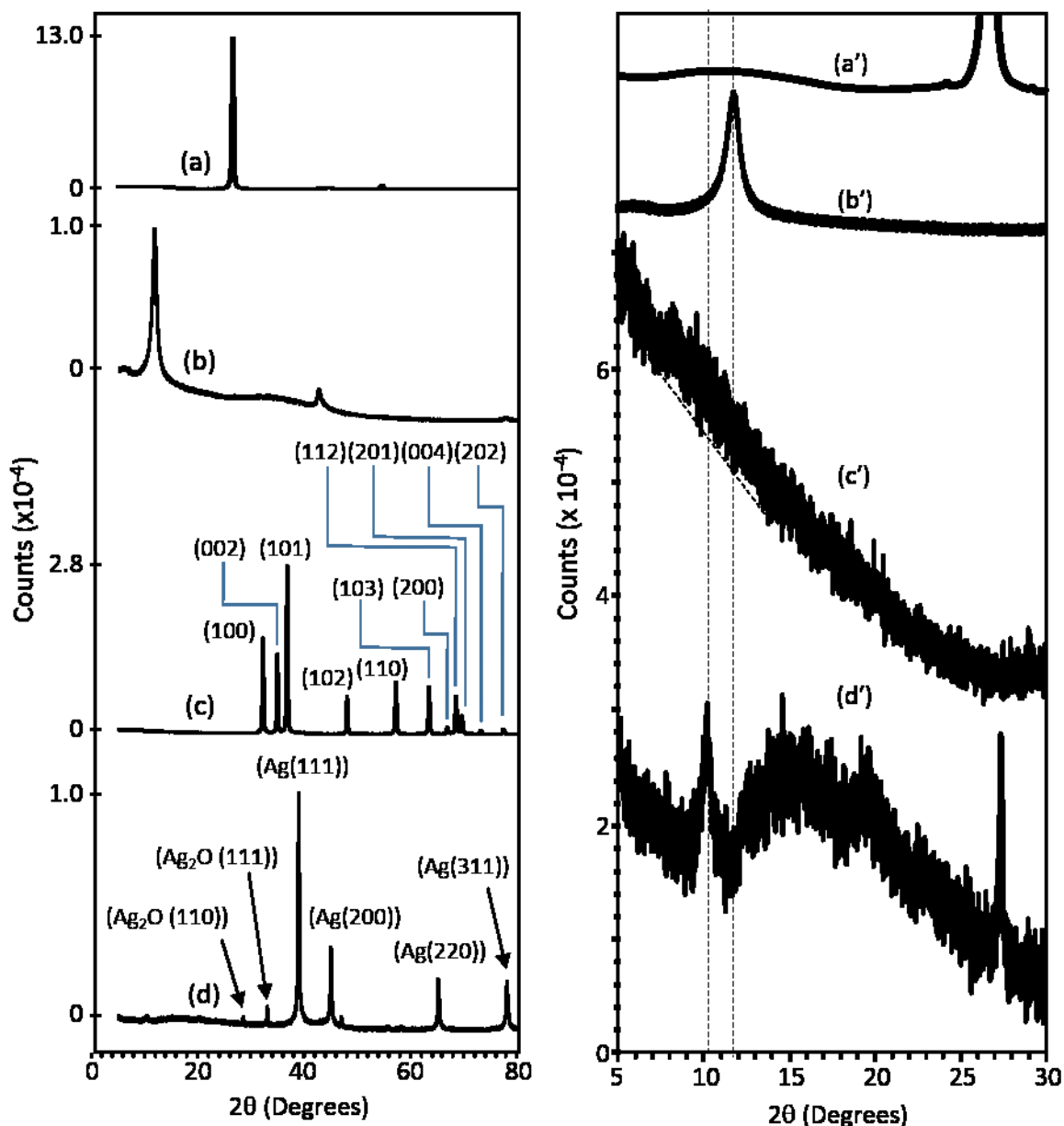
510 Unwin, P.R., Guell, A.G., Zhang, G.H., 2016. Nanoscale Electrochemistry of sp² Carbon
511 Materials: From Graphite and Graphene to Carbon Nanotubes. *Accounts of Chemical*
512 *Research* 49, 2041-2048.

513 Wang, D., An, J., Luo, Q., Li, X., Yan., L 2012. Nano Antimicrobials. Springer, London
514 New York.

515 Xie, Y., He, Y., Irwin, P. L., Jin, T., Shi, X., 2011. Antibacterial activity and mechanism of
516 action of zinc oxide nanoparticles against *Campylobacter jejuni*. Applied of Environmental
517 Microbiology 77, 2325-2331.

518 Zhou, J., Zhao, F., Wang, Y., Zhang, Y., Yang, L., 2007. Size-controlled synthesis of ZnO
519 nanoparticles and their photoluminescence properties. Journal of Luminescence 122, 195-197.

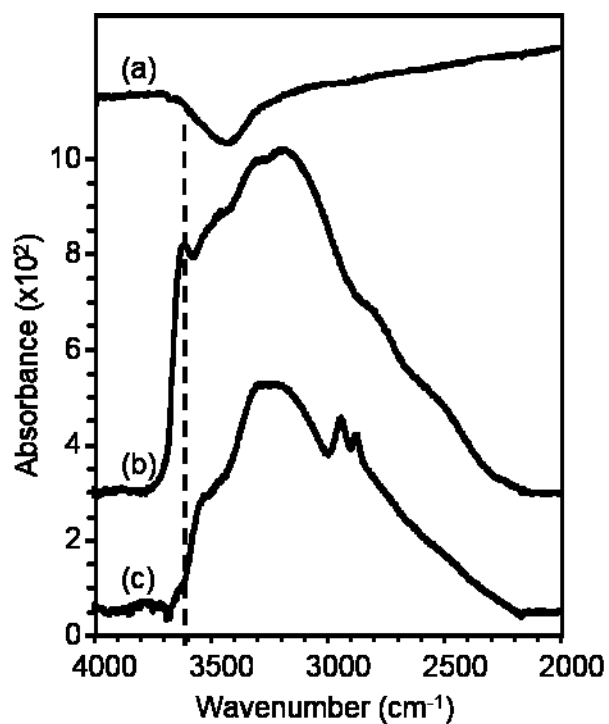
520



521

522 **Fig. 1** X-Ray Diffraction patterns for; (a) graphite, (b) graphene oxide (GO), (c) zinc oxide – graphene
 523 oxide hybrid (ZnOGO) and (d) silver – graphene oxide hybrid (AgGO). Note the individual peak heights
 524 – patterns have been compressed to fit. In the right hand stack, patterns a' to d' correspond to those
 525 in the left stack but are plotted over a narrower 2θ range on common counts scale (with Y-shifting for
 526 presentation purposes). ZnOGO and AgGO have 50 x boosted counts and are Y-shifted for presentation
 527 purposes.

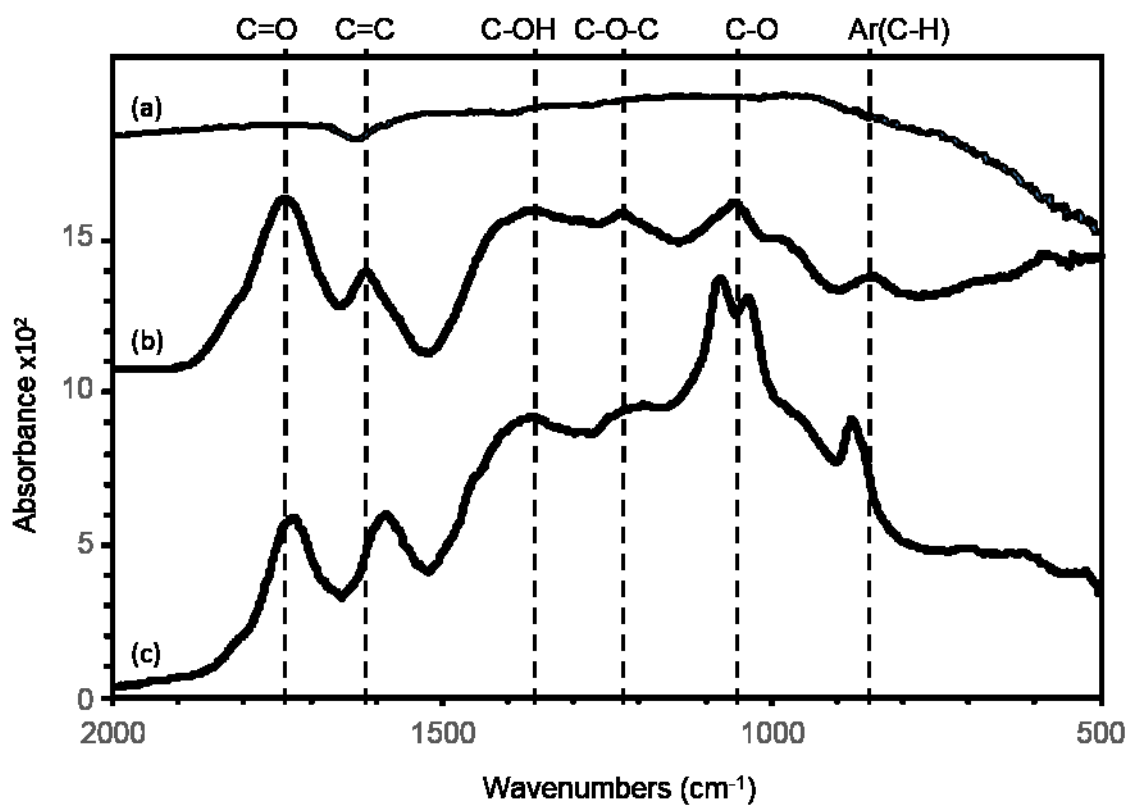
528



529

530 **Fig. 2** DRIFTS spectra (4000 cm⁻¹ to 2000 cm⁻¹) of (a) graphite, (b) graphene oxide (GO) and (c) silver –
531 graphene oxide hybrid (AgGO).

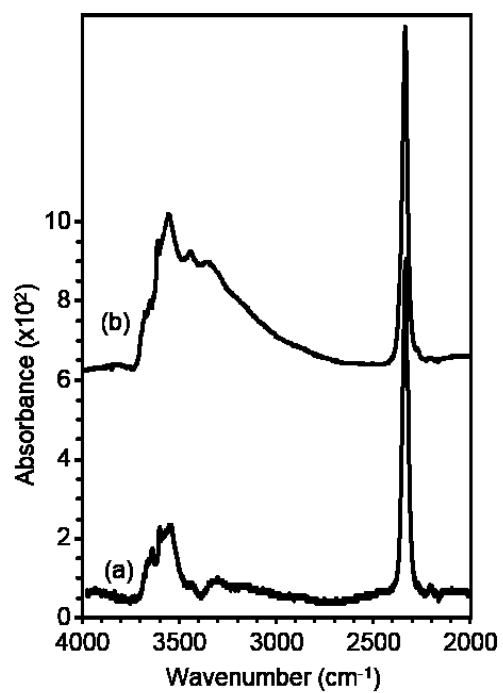
532



534

535 **Fig. 3** DRIFTS spectra (2000 cm⁻¹ to 500 cm⁻¹) of (a) graphite, (b) graphene oxide (GO) and (c) silver –
536 graphene oxide hybrid (AgGO).

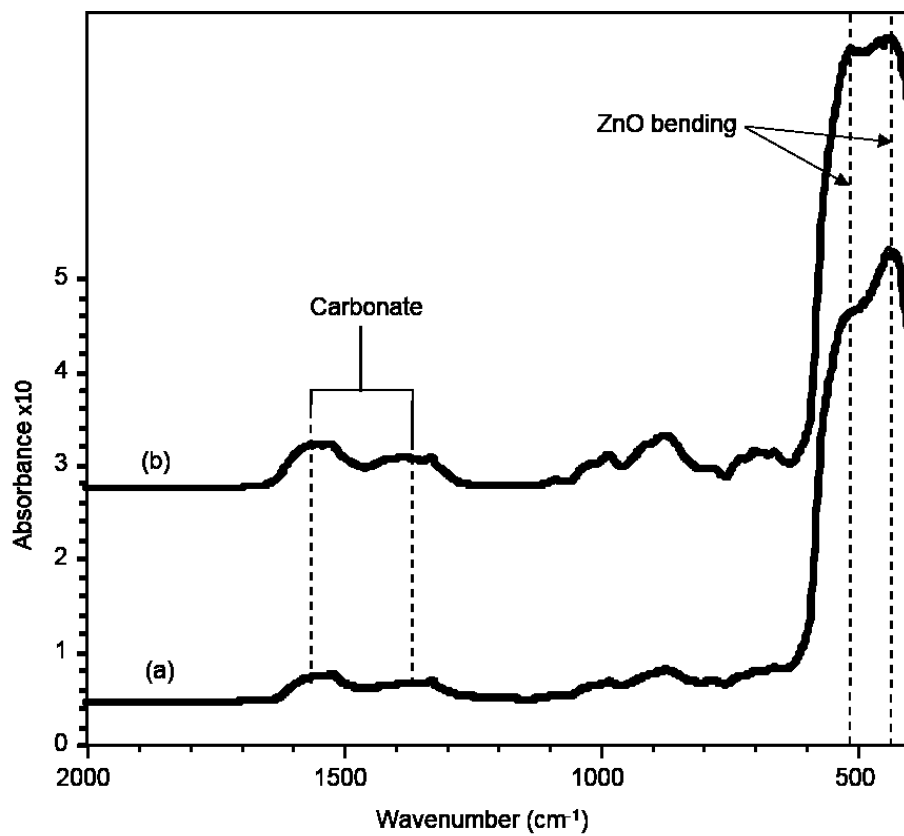
537



538

539 **Fig. 4** DRIFTS spectra (4000 cm⁻¹ to 2000 cm⁻¹) of (a) synthesised zinc oxide (ZnO), (b) synthesised zinc
540 oxide – graphene oxide hybrid (ZnOGO).

541

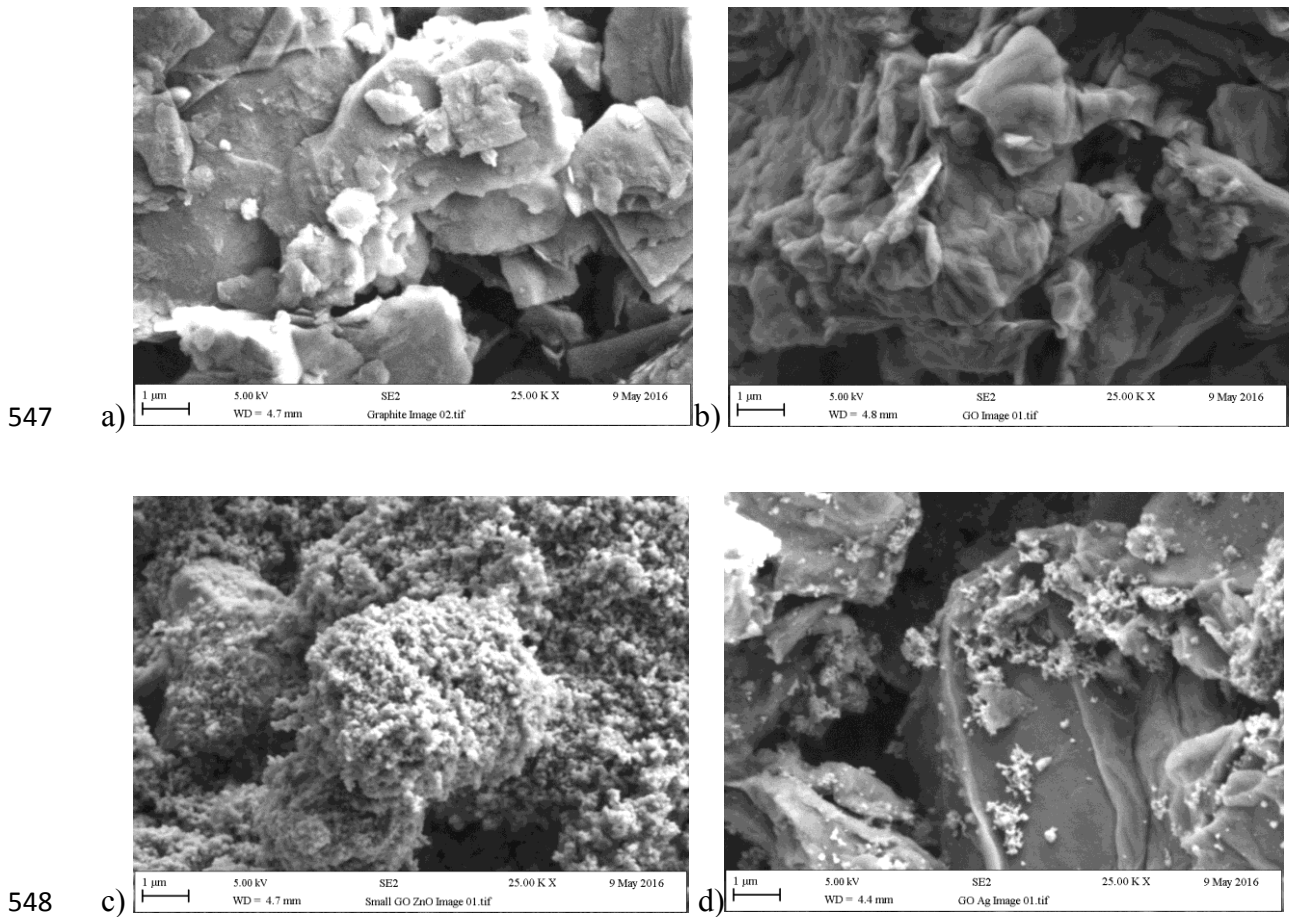


542

543 **Fig. 5** DRIFTS spectra (2000 cm⁻¹ to 400 cm⁻¹) of (a) synthesised zinc oxide (ZnO), (b) synthesised zinc
544 oxide – graphene oxide hybrid (ZnOGO).

545

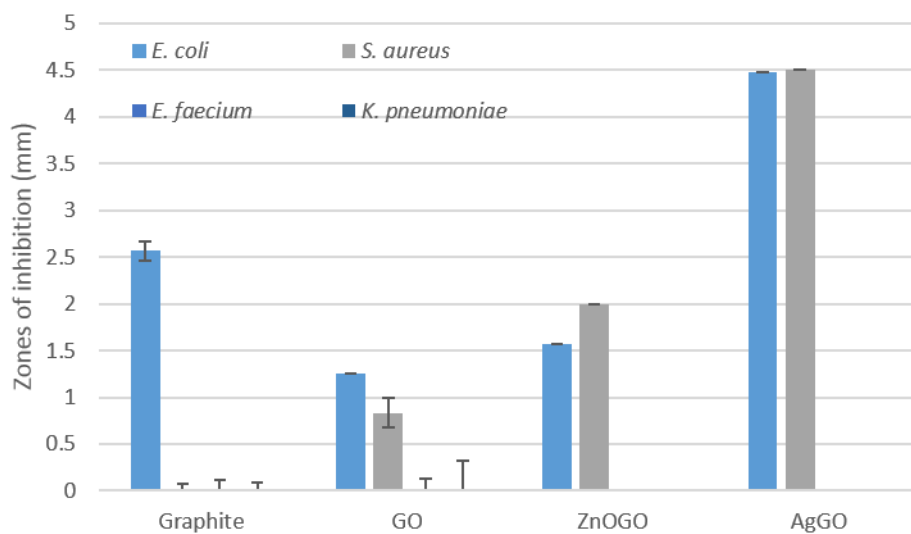
546



549 **Fig. 6** SEM images demonstrating the morphology and particle sizes of a) graphite, b) graphene oxide
550 (GO), c) zinc oxide – graphene oxide hybrid (ZnOGO) and d) silver – graphene oxide hybrid (AgGO).

551

552

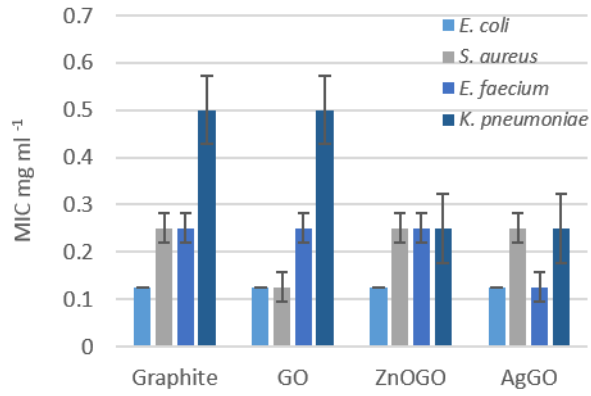


553

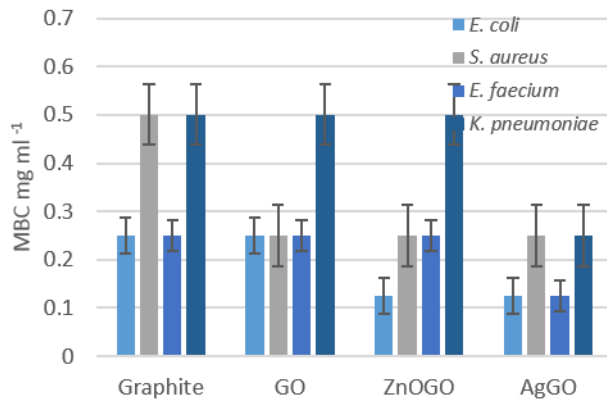
554 **Fig. 7** Zone of inhibition measurements demonstrating the antimicrobial efficacy of the compounds.
555 The silver – graphene oxide hybrid (AgGO) was determined to be the most effective antimicrobial
556 using this method. *K. pneumoniae* and *E. faecium* did not demonstrate inhibition by the compounds
557 using this method.

558

559



560



561

562 **Fig. 8** a) MIC and b) MBC of compounds against the four medically relevant bacteria demonstrating
 563 that the silver – graphene oxide hybrid (AgGO) demonstrated the greatest inhibitory and bactericidal
 564 effect.

565

566 Table 1 EDX analysis demonstrating the elemental analysis (% weight) of the compounds

	C	O	Ag	Zn
Graphite	91.12 ± 0.13	8.88 ± 0.13	N/A	N/A
GO	54.15 ± 0.79	45.85 ± 0.79	N/A	N/A
ZnOGO	8.60 ± 0.04	18.75 ± 0.17	N/A	72.65 ± 0.13
AgGO	14.50 ± 1.50	15.74 ± 1.03	69.77 ± 2.53	N/A

567 N/A Not applicable for elemental analysis

568

569

570 Table 2 Effect of silver addition on infrared absorption frequencies

Group vibration	Vibration frequency (cm ⁻¹)		Dn (cm ⁻¹)
	GO	Ag-GO	
C=O	1738	1728	-10
C=C	1615	1586	-29
C-OH	1356	1363	+7
C-O-C	1225	1220	-5
C-O	1056	1078	+22
		1037	-19
Aromatic C-H	849	879	+30

571

572

573 Table 3 Minimum to maximum size range of the particles

574

	Smallest size (μm)	Greatest size (μm)
Graphite	0.10	25.7
Graphene oxide	0.20	20.0
ZnOGO	0.05	30.0
AgGO	0.01	13.0

575

576

577